

pubs.acs.org/Macromolecules Article

Electrospinning Fibers from Oligomeric Complex Coacervates: No Chain Entanglements Needed

Xiangxi Meng, Yifeng Du, Yalin Liu, E. Bryan Coughlin, Sarah L. Perry,* and Jessica D. Schiffman*



Cite This: Macromolecules 2021, 54, 5033-5042



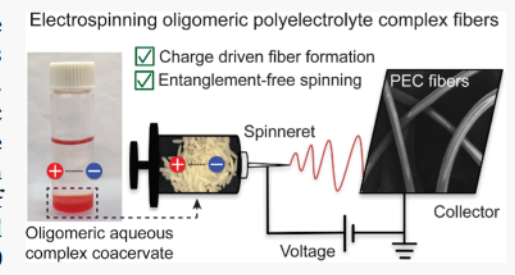
ACCESS I

III Metrics & More

Article Recommendations

Supporting Information

ABSTRACT: The electrospinning field is dominated by studies that investigate parameters, such as polymer concentration and chain length, to identify conditions where the polymer chains are sufficiently entangled to facilitate fiber formation. Here, we report the first demonstration that linear, nonentangled, oligomeric polyelectrolytes can be electrospun into fibers using a traditional single-nozzle setup. Previously, we have demonstrated that the associative phase separation phenomenon known as complex coacervation facilitates the electrospinning of polyelectrolyte complex fibers directly from water. In this work, we synthesized polycations and polyanions with degrees of polymerization ranging from ~500 down to <10, representing average molecular weights on the order of 100 to 1 kg/



mol. We then quantified the phase behavior and viscosity of our various coacervate samples as a function of both chain length and salt concentration. Our results confirm that the polymer concentration in all samples was near or above the estimated value for the overlap concentration and that only the longest polymer samples were expected to experience entanglements. However, we were able to electrospin fibers from all of our coacervate samples, even oligomers. Thus, the electrospinnability of coacervates is fundamentally different from the traditional electrospinning of linear, neutral polymers or solutions composed of polyelectrolytes mixed with neutral polymers. In the same way that coacervation represents a novel way to enable the electrospinning of polyelectrolytes from water, the associative interactions driving phase separation eliminate the need for entanglements by slowing the timescale for relaxation. Our results suggest an alternative route that enables the electrospinning of novel solutions by decoupling chain-length requirements from other length-dependent parameters.

■ INTRODUCTION

Electrospinning is a convenient, well-established technique to manufacture nonwoven mats comprised of micro- and nanoscale fibers that have a large surface-to-volume ratio.1 Electrospun fiber mats are multifunctional materials that can be produced using a scalable process²⁻⁴ and are widely used in tissue engineering, 5-7 separations, 8,9 and battery applications. 10,11 While fibers have been electrospun from over 100 different polymers,12 electrospinning has been limited to relatively long polymers.

Electrospinning utilizes electrical forces to drive the formation of fine fibers. 13,14 Specifically, an applied voltage induces charges in the precursor solution to first form a Taylor cone at the tip of the spinneret. 15,16 The electric field then pulls the polymer solution from the Taylor cone, creating a jet that accelerates toward the collector plate. During flight, the jets are further thinned into fibers with micro- or nanometerscale diameters due to intense whipping and bending instabilities. 14-20 To avoid the formation of droplets during flight, electrospinning has typically relied on the physical entanglement of polymers in the electrospinning solution to slow chain rearrangement and suppress capillary instabilities.

The need to prepare an entangled polymer solution places a lower bound on both the concentration and the length of the polymers that can be used. Classical polymer physics describes

a critical entanglement molecular weight (M_C) , usually in the range of 10-20 kg/mol for polymers, which indicates the minimal length for a polymer to entangle in a solution or melt.21-23 The concentrations where polymers begin to overlap and entangle are defined as the overlap concentration (C^*) and entanglement concentration (C_e) , respectively, with longer polymers entangling at lower concentrations. As relates to electrospinning, empirical evidence has suggested that smooth, continuous fiber formation requires concentrations significantly above this entanglement threshold, such that C_{fiber} $\sim 4 \times C_{\rm e}^{24-31}$

One consequence of this reliance on physical entanglements is the inability to electrospin polymers below Ce, whether as a result of a low degree of polymerization (N) and/or low polymer concentrations (Cp) in solution. For example, the shortest polymer we found in the literature, which was electrospun from an entangled aqueous solution, was the short-

Received: February 18, 2021 Revised: April 21, 2021 Published: May 17, 2021





chain, neutral polymer poly(vinyl alcohol) (PVA, 9–10 kg/mol, $N \sim 200-230$). There are alternative strategies to enable the electrospinning of polymer solutions without relying on entanglements; they aim to slow the relaxation time of the polymers in the solution. For example, to facilitate the electrospinning of a very short poly(4-vinylpyridine) (P4VP, 5.2 kg/mol, $N \sim 50$), it was necessary to include a hydrogenbonding additive, 4,4'-biphenol. On the other hand, the electrospinning of very long neutral polymers below the entanglement concentration has been demonstrated by adding small amounts of a hyperbranched polymer that slowed the relaxation time of the solution. Studies have also shown that self-associating molecules, such as cyclodextrin and tannic acid, can be electrospun into continuous fibers.

While the electrospinning of charged polymers has typically suffered from challenges associated with the self-repulsion of charges along the polymer chain, coacervation is an associative liquid-liquid phase separation phenomenon that takes advantage of complexation between oppositely charged polymers to produce a largely charge-neutral solution, similar to a neutral polymer solution. Furthermore, the ionpairing interactions that drive coacervation provide stability after fiber formation, eliminating the need for chemical crosslinking or post-processing. Previously, our team has demonstrated that complex coacervation can enable the electrospinning of polyelectrolytes from water. 44-46 Our work on electrospinning coacervates took advantage of relatively highmolecular-weight polymers that were physically entangled at the concentrations present in the coacervate, i.e., poly(4styrene sulfonic acid, sodium salt) (332 kg/mol, $N \sim 1800$) and poly(diallyldimethylammonium chloride) (400 kg/mol, N ~ 2500), 44,45 as well as a biopolymer system formed from hyaluronic acid (199 kg/mol, $N \sim 500$) and chitosan (50–190 kg/mol, $N \sim 300-1100$). However, the aforementioned reports describing the electrospinnability of associating small molecules inspired us to explore the potential for using the associative interactions that drive phase separation to enable the electrospinning of coacervates formed from oligomers.

In this work, we demonstrate that the associative interactions that drive complex coacervation can circumvent the need for physical entanglements and enable the electrospinning of oligomers. To achieve this goal, we prepared coacervates from a series of anionic poly(3-sulfopropyl methacrylate potassium salt) (PSPMA) and cationic poly([2-(methacryloyloxy)ethyl]trimethylammonium iodide) (PTMAEMA) polymers with different molecular weights (Figure 1a). This series of structurally similar methacryloyl polyelectrolytes allowed us to correlate coacervate phase behavior with electrospinnability as a function of polymer chain lengths, spanning the range from a physically entangled coacervate to one formed from unentangled oligomers.

MATERIALS AND METHODS

Materials. All reactants, 3-sulfopropyl methacrylate potassium salt (SPMA, 98%, Sigma-Aldrich), 2-(dimethylamino)ethyl methacrylate (DMAEMA, 98%, Sigma-Aldrich), iodomethane (99%, Sigma-Aldrich), 4-cyano-4-(phenylcarbonothioylthio) pentanoic acid (Sigma-Aldrich), 4,4'-azobis(4-cyanovaleric acid) (ACVA, Sigma-Aldrich), dioxane (anhydrous, 99.8%, Sigma-Aldrich), acetone (ACS grade, Fisher Scientific), tetrahydrofuran (THF, ACS grade, Fisher Scientific), diethyl ether (ACS grade, Fisher Scientific), and potassium bromide (KBr, ACS grade, Fisher Scientific), were used as received. Deionized (DI) water was obtained from a Milli-Q water purification system (resistivity of 18.2 MΩ cm, Millipore).

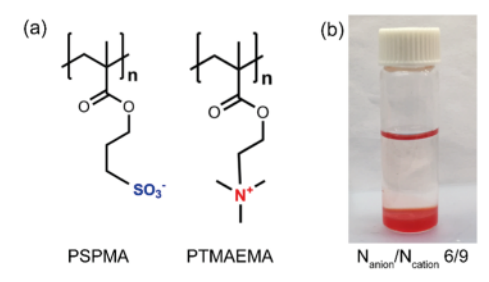


Figure 1. (a) Chemical structures of poly(3-sulfopropyl methacrylate) (PSPMA) and poly([2-(methacryloyloxy)ethyl]trimethylammonium) (PTMAEMA), chosen as a set of structurally similar, methacryloylbased polyelectrolytes. Counterions of potassium and iodide were omitted from the chemical structures for simplicity. (b) Photograph of a coacervate sample prepared from oligomeric PSPMA and PTMAEMA with $N_{\rm anion}/N_{\rm cation}=6/9$ and no added salt. The dense, polymer-rich coacervate phase appears red due to the presence of the phenylcarbonothioylthio group from the chain-transfer agent (CTA). The coacervate was isolated from the polymer-poor supernatant before electrospinning.

Cationic Monomer Synthesis. Monomers for the polycation were prepared by the quaternization of commercially available 2-(dimethylamino)ethyl methacrylate (DMAEMA) (Figure S1a). DMAEMA (15 g, 95.4 mmol) was first dissolved in THF (150 mL, dry) in a flask submerged in an ice bath, followed by degassing with nitrogen for 1 h. An excess of iodomethane (27.1 g, 190.1 mmol) was then added dropwise into the solution. The resulting mixture was stirred under nitrogen gas for 1.5 h in the ice bath and then allowed to react further at room temperature for 24 h. The product, [2-(methacryloyloxy)ethyl]trimethylammonium iodide (TMAEMA), precipitated out of solution and was filtered and rinsed with diethyl ether before drying under vacuum overnight. The successful quaternization reaction reached 99% conversion of DMAEMA, determined by ¹H NMR (Figure S1b).

Polymer Synthesis and Characterization. All polymers used in this work were synthesized by reversible addition-fragmentation chain-transfer (RAFT) polymerization⁴⁷ (Figure S2). RAFT was chosen because of the ability to precisely control the molecular weight of polymers from monomers of various chemical functionalities under different reaction conditions. $^{47-50}$ The targeted degrees of polymerization were $N \sim 500$, 50, 20, and 5 for both the polyanion and the polycation. 4-Cyano-4-(phenylcarbonothioylthio) pentanoic acid was used as a chain-transfer agent (CTA) and 4,4'-azobis(4-cyanovaleric acid) (ACVA) was used as the initiator in all reactions at a molar ratio of 10:1 (CTA/initiator). The degree of polymerization (N) was tuned by modulating the feed ratio between the monomer and the CTA/ initiator. Each polymer was synthesized at a total polymer scale of 5 g. All reactants were added to a 50 mL Schlenk flask under a nitrogen atmosphere. For the synthesis of polymers with chain length $N \ge 50$, only water was used as a solvent. For short-chain batches (N = 5 and 20), ~10 mL of dioxane was used as the co-solvent with water to modulate the polarity of the solvent to account for the high concentrations of the chain-transfer agent (CTA) and initiator, which have limited solubility in water. Three cycles of freeze/pump/thaw were applied to degas the solution. The Schlenk flask was then backfilled with nitrogen and placed in an oil bath at 70 °C. The reaction was kept at 70 °C for 14 h for polymers with $N \ge 50$. The reaction time was shortened to 6 h for the synthesis of shorter polymers (N = 5 and 20) to achieve a similar monomer conversion level, as well as to minimize potential side reactions, such as CTA hydrolysis due to the relatively high CTA concentration. The polymerization was quenched by immersing the flask into an ice bath. The product solution was precipitated into acetone to yield the solid polymer product, which was redissolved in water and precipitated in acetone three times to remove excess reactants. The resultant polymer products, poly(3-sulfopropyl methacrylate potassium salt) (PSPMA) and poly([2-(methacryloyloxy)ethyl] trimethy-

lammonium iodide) (PTMAEMA), were then dried under vacuum before further use.

Proton nuclear magnetic resonance spectroscopy (1 H NMR, Bruker Avance III 500) was performed in 5 mm diameter tubes in deuterated water (D_2O) at 25 °C. The monomer conversion for the polymerization reactions was ~80%, calculated from 1 H NMR of the crude polymerization solutions, based on a comparison of the integrated peak areas of the hydrogens from the alkene of the monomer and those of the polymer. The degree of polymerization (N) and the number average molecular weight (M_N) were determined based on end-group analysis from 1 H NMR spectra (Figure S3). Table 1 summarizes N and M_N of all PSPMA and PTMAEMA used in this study.

Table 1. Average Degrees of Polymerization (N) and Number Average Molecular Weights $(M_N, g/mol)$ for PSPMA and PTMAEMA, Determined by End-Group Analysis from ¹H NMR

	N	$\frac{M_{ m N}}{({ m g/mol})}$	$M_{ m N}$ without counterion (g/mol)
polyanion (PSPMA) ^a	6	1478	1243
	18	4434	3730
	45	11 084	9325
	450	110 844	93 250
polycation (PTMAEMA) ^b	9	2692	1550
	23	6881	3962
	47	14 061	8096
	470	140 605	80 960

^aThe counterion for PSPMA was potassium. ^bThe counterion for PTMAEMA was iodide.

Complex Coacervate Preparation and Characterization. Polyelectrolyte stock solutions were prepared gravimetrically at a concentration of 0.125 M on a monomer basis in DI water. A stock solution of KBr was also prepared gravimetrically at a concentration of 2.0 M using DI water.

Complex coacervates were prepared by adding KBr solution, water, polyanion, and polycation solutions sequentially into a centrifuge tube. The mixture was vortexed for 60 s between the addition of each solution to ensure good mixing. The molar ratio of the cation to anion (on a monomer basis) was fixed at 1:1 for all samples. Different scale samples were prepared for binodal phase diagrams, rheology experiments, and electrospinning. For binodal phase diagrams, microcentrifuge tubes (2 mL, Fisher Scientific) were used with a total sample volume of 1.5 mL. For rheology and electrospinning experiments, large centrifuge tubes (50 mL Falcon, Fisher Scientific) were used with a total sample volume of 50 mL. All samples were prepared with a total initial C_p of 45 mM, on a monomer basis, and then mixed overnight on a tube rotator (Arma-Rotator A-1, Elmeco Engineering) at 20 rpm to allow the sample to fully equilibrate. To coalesce the dense coacervate phase, microcentrifuge tubes were centrifuged at 17 000g (13 300 rpm, Sorvall Legend Micro 17 Centrifuge, Thermo Fisher Scientific) for 20 min, while larger centrifuge tubes were centrifuged at 4000g (10000 rpm, Sorvall ST 16R Centrifuge, Thermo Fisher Scientific) for 20 min.

A descriptive weight average molecular weight $(M_{W,coacervate}^*)$ and number average molecular weight $(M_{N,coacervate}^*)$ of the coacervates based on the size of the polymers used in each sample are tabulated in Table S1. The mathematical equations for both $M_{W,coacervate}^*$ and $M_{N,coacervate}^*$ are provided in eqs 1 and S1, respectively. The living character of the RAFT polymerization technique confers narrow dispersities to the resultant polymers; therefore, the number average molecular weights (M_N) of PSPMA and PTMAEMA were used in these calculations, neglecting the inherent dispersity of each polymer sample. The counterions of the polyelectrolytes were omitted, *i.e.*, potassium ion for PSPMA and iodide for PTMAEMA, due to counterion release during coacervation. In this work, $M_{W,coacervate}^*$ was

used since it is a more common parameter for a polymer blend with the sensitivity of molecular size rather than $M_{N,\text{coacervate}}^*$, which is sensitive to polyanion and polycation proportional molarity.

$$M_{\text{W,coacervate}}^* = \frac{M_{\text{N, pSPMA}}^2 + M_{\text{N, PTMAEMA}}^2}{M_{\text{N, pSPMA}} + M_{\text{N, pTMAEMA}}}$$
(1)

A combination of turbidimetry and visual inspection by optical microscopy was used to determine the salt resistance of each coacervate system. Samples of 200 µL at a total polymer concentration (C_p) of 20 mM (on a monomer basis) were first prepared in a 96-well plate (Falcon, Fisher Scientific) and three samples of 50 µL were then transferred to a 384-well plate. The turbidity of each sample was measured in triplicate using a microplate reader (BioTek Synergy H1) at a wavelength of 562 nm (Figure S4). Turbidity was defined as the natural log of the ratio between the intensity of the incident light and the intensity of light passing through the sample and was measured in absorbance units. An optical microscope (EVOS FL Auto) with a 40× objective was used to visually inspect samples immediately after preparation and allow for the identification of the formation of a precipitate, coacervate, and/or the absence of phase separation. Additionally, control samples were made from a mixture of the SPMA and TMAEMA monomers, as well as each of the polyelectrolyte monomers. The salt resistance was defined as the concentration of salt above which no phase separation was observed (Figures S4 and S5).

Phase Diagram Determination. The salt concentration (C_S) in the supernatant was measured via conductivity (Oakton Con 450) and referenced against potassium bromide (KBr) and counterion potassium iodide (KI) calibration curves (Figure S6). The C_P in both supernatant and coacervate phases was measured by precipitating each phase in 10 mL of ethanol three times. Ethanol was chosen because of the relatively high solubility of KBr in this solvent. The precipitated solids were then lyophilized overnight to remove ethanol and weighed. The volume of the supernatant was measured using a 100 mL glass volumetric cylinder, and the coacervate volume was determined by subtracting this measured supernatant volume from the total conserved volume of 50 mL. Experiments were conducted in triplicate. The C_S in the coacervate was then calculated via mass balance based on the measured values from the supernatant.

Linear Viscoelasticity Characterization of Complex Coacervates. Rheology measurements were performed using a Malvern Kinexus Pro stress-controlled instrument, run in strain-controlled oscillatory mode. A 20 mm diameter stainless parallel plate fixture was used for the shortest-chain (N_{anion}/N_{cation}) of 6/9 coacervates, with a gap size of 1 mm. A cone-plate fixture (50 mm diameter, 0.2°) was used for all other samples (gap size = 0.07 mm). During all experiments, a solvent trap was used with mineral oil to prevent water evaporation. Before running frequency sweeps, an amplitude sweep measurement at 6.28 Hz was conducted to assure that the strain amplitude used (between 0.5 and 1.0%) was within the linear viscoelastic regime for each coacervate sample. The storage and loss moduli (G' and G'') were measured as a function of angular frequency from 100 to 0.1 rad/s. Data points with large errors (i.e., harmonic distortion >5%) were removed to ensure data quality. The zero-shear viscosity of the coacervates was extrapolated from the frequency sweep data using IRIS software. 51 All experiments were conducted in duplicate at 25 °C to ensure reproducibility. The statistical analysis on the slopes of coacervate viscosity dependence on Cp was performed on all N combinations based on a two-tailed, Student's t-test with p <

Theoretical Calculations of the Overlap and Entanglement Concentrations. The theoretical overlap concentration (C^*) , entanglement concentration (C_e) , and condition for the onset of fiber formation (C_{fiber}) were estimated for poly(methyl methacrylate) (PMMA, monomer $M_W = 100.1$ g/mol) as a structurally similar and well-characterized neutral polymer. The Kuhn molecular weight $(M_{W, \text{Kuhn}})$ of PMMA is 655 g/mol. Thus, the Kuhn segment (N_K) for PMMA was calculated to contain 6.5 repeat units and was used to calculate C^* , C_e , and C_{fiber} . We assumed the PMMA model in θ

solvent (excluded volume = 0), as the polyelectrolyte chains in the aqueous coacervates have been previously shown to have a Gaussian coiled polymer geometry. The number of $N_{\rm K}$ for each coacervate was extrapolated with respect to the average $M_{\rm W,coacervate}^*$ of each coacervate. Therefore, C^* was estimated as 52

$$C^* \sim N_{K}^{-0.764} \tag{2}$$

with an entanglement concentration (Ce) of approximately

$$C_{\rm e} \approx 10 \times C^*$$
 (3)

Electrospinning of Complex Coacervates. After centrifugation, the dense coacervate phase was loaded into a 5 mL Luer-Lock tip syringe capped with a PrecisionGlide 22-gauge needle (BD). The syringe was secured to a PHD ultra syringe pump (Harvard Apparatus). Alligator clips were used to connect the positive anode of a high-voltage supply (Gamma High Voltage Research Inc.) to the needle, while the negative anode was connected to a copper plate wrapped in an aluminum foil. For all experiments, the coacervate was fed at a constant advancement rate of 1.0 mL/h, an applied voltage of 14 kV, and a needle-to-collector plate separation distance of 15 cm, based on our previous work. 44,45 The electrospinning apparatus was housed in an environmental chamber (CleaTech) maintained at a temperature of 23 \pm 1 °C and a relative humidity of 25-27% using a desiccant unit (Drierite). All coacervates were electrospun for 20 min before examination using an FEI-Magellan 400 scanning electron microscope (SEM). A Cressington high-resolution ion beam coater model 108 was used to sputter coat samples for 120 s with gold.

■ RESULTS AND DISCUSSION

The goal of this study was to investigate whether the associative electrostatic interactions that drive complex coacervation are sufficient to enable the electrospinning of unentangled coacervates formed from oligomers. We used controlled radical polymerization to make low polydispersity, oppositely charged polyelectrolytes that could form coacervates. Specifically, we selected a pair of methacryloyl-based polyelectrolytes (Figure 1) as our model system to maintain a constant polymer backbone and similar side-chain structure for both the anionic and cationic species. We then characterized the phase behavior and linear viscoelasticity of our coacervate system as a function of the degree of polymerization (N) and salt concentration (Cs) and combined these fundamental solution studies with electrospinning experiments and microscopy analysis. In this work, we will refer to our various coacervate samples based on the chain lengths of the two polymers involved (i.e., $N_{\text{anion}}/N_{\text{cation}}$).

Coacervate Phase Behavior. To begin with, we characterized the phase behavior of our various polymer samples as a function of added KBr concentration (C_S) , as displayed in Figures 2, S4, and S5. Complexes of our methacryloyl polymers behaved as "saloplastic" materials, $^{53-55}$ forming solid precipitates at low C_S , liquid—liquid phase-separated complex coacervates at intermediate C_S , and ultimately transitioning to a single phase at high C_S . Furthermore, an increase in the polymer chain length led to both an increased tendency for solid precipitation (Figure S4) and persistence of liquid coacervates at higher C_S and C_P (Figures 2a and S5), as expected. $^{47,56-61}$ In fact, precipitation was observed for all of our systems, except for the shortest $N_{\rm anion}/N_{\rm cation} = 6/9$ system (Figure S4a).

The driving force for complex coacervation is generally attributed to the large entropic gains associated with the release of bound counterions from the individual polymers upon complex formation. 56,57,59,60,62-66 In particular, this localization of counterions (*i.e.*, Manning condensation)⁶⁷ is

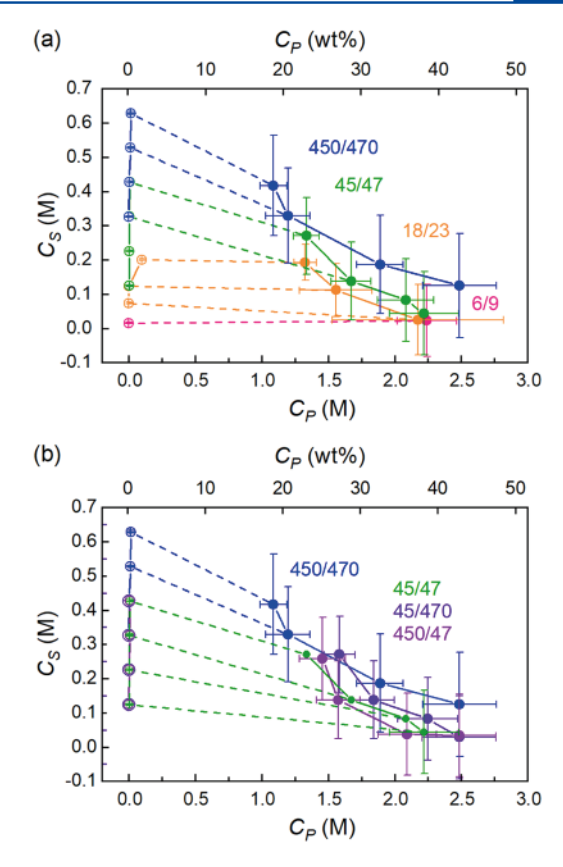


Figure 2. Experimentally determined polymer—salt phase diagrams for the complex coacervation of (a) length-matched PSPMA and PTMAEMA showing the effect of increasing the chain length with $N_{\rm anion}/N_{\rm cation}$ of 6/9, 18/23, 45/47, and 450/470 and (b) length-mismatched polymers with $N_{\rm anion}/N_{\rm cation}$ of 45/470, and 450/47. Tie lines connect data for corresponding coacervate (closed symbols) and supernatant (open symbols) samples. $C_{\rm P}$ is on a monomer basis. Error bars are based on the uncertainty of measurement and propagation of

facilitated by the high charge density of the polymer chain and is weaker at the ends of a polymer chain. This "end effect" helps to explain the observed decrease in the stability of a coacervate as the polymer chains decrease in length and the end effects become more significant.⁵⁷ Furthermore, loss of sufficient counterion condensation in the limit of very short chains would be expected to eliminate the driving force for coacervation. Our results are consistent with other reports that included studies of coacervation as a function of chain length. 47,57-60,68 While a lower limit with respect to chain length has not been rigorously explored in the literature, examples exist where, for example, length-matched 12-mer polypeptides of poly(lysine) and poly(glutamate)⁵⁷ and a system of adenosine triphosphate (ATP) with a 10-mer of poly(lysine)⁶⁹ formed coacervates. However, the ability for our system to form coacervates from oligomers with $N_{\rm anion}/N_{\rm cation}$ of 6/9 was not necessarily expected. To test the limits of phase separation, we also performed a control experiment where oppositely charged methacryloyl monomers were mixed. However, no phase separation was observed by optical

The phase diagrams in Figure 2 highlight the interplay between C_P and C_S in the coacervate phase. A sample prepared at a concentration that falls under the binodal curve will phase separate into a polymer-rich coacervate and a polymer-poor

supernatant along a tie line. The thermodynamic equilibrium described by this tie line complicates the preparation of samples with different $C_{\rm P}$ values for use in electrospinning experiments, where $C_{\rm P}$ has traditionally been a key adjustable parameter to control the spinnability and the size of the resulting fibers. While it is straightforward to simply prepare a more concentrated solution by adding more polymers, a coacervate sample that is prepared at a higher $C_{\rm P}$ on the same tie line would simply produce a greater volume of the same coacervate, rather than a coacervate with higher $C_{\rm P}$. However, with the knowledge of the phase behavior of our various polymer systems, we can prepare samples with a specified coacervate composition for comparison across different N values.

While a detailed analysis of the phase behavior of this system has been published elsewhere, briefly, we were able to prepare coacervates of different N values in the same general range of $C_{\rm P}$. Oligomeric coacervates of $N_{\rm anion}/N_{\rm cation}$ 6/9 were formed without the addition of salt at a $C_{\rm P}$ of 2.2 M. With increasing chain length, it was necessary to increase $C_{\rm KBr}$ to 0.05, 0.1, and 0.3 M to maintain the same $C_{\rm P}$ for N 18/21, 45/47, and 450/470, respectively. As N increases, the width of the two-phase region also increased (Figure 2), in agreement with previous reports and theoretical predictions.

We were also inspired by previous reports in the electrospinning literature where a long polymer was used as a carrier to facilitate entanglements and the electrospinning of a shorter polymer. 31 Therefore, we explored the coacervation of polymers with mismatched N. We hypothesized that our longest-chain length $N \sim 500$ polymers would have the potential to entangle, while our shorter ~50-mers would not. This is an analogous approach to the use of a longer carrier polymer to facilitate the electrospinning of an otherwise unspinnable polymer, as has been commonly reported in the electrospinning literature. Therefore, we prepared coacervates from polymers with mismatched chain lengths $N_{\rm anion}/N_{\rm cation}$ of 45/470 and 450/47. Interestingly, Figure 2b shows that the phase behavior of these length-mismatched polymers was dominated by the shorter polyelectrolyte. A detailed theoretical and rheological analysis of these effects has been published elsewhere,⁴⁷ but briefly the dominance of the shorter polymers on the phase behavior has been attributed to a loss of translational entropy from the larger number of short polymers needed to form a complex with a single longer polymer. The dominating impact from shorter polymer species on the phase behavior of length-mismatched systems was further confirmed by two control experiments. No phase separation was observed when mixing two oppositely charged monomers together, nor was when mixing a long-chain polymer ($N \sim 500$) with the oppositely charged monomer.

Coacervate Viscoelasticity. Next, we wanted to determine the presence or absence of physical entanglements based on our knowledge of the coacervate phase behavior. Traditionally, the onset of entanglement has been observed *via* rheology. Polymeric electrospinning precursor solutions are conventionally characterized by measuring viscosity as a function of C_P using a log-log plot. While increasing C_P would generally lead to an increase in solution viscosity, the presence of entanglements can dramatically accelerate this trend.²³ Therefore, a sharp increase in the slope on a log-log plot of viscosity ν s C_P is indicative of entanglements, with the critical C_P defined as C_e (Figures 3 and S7).

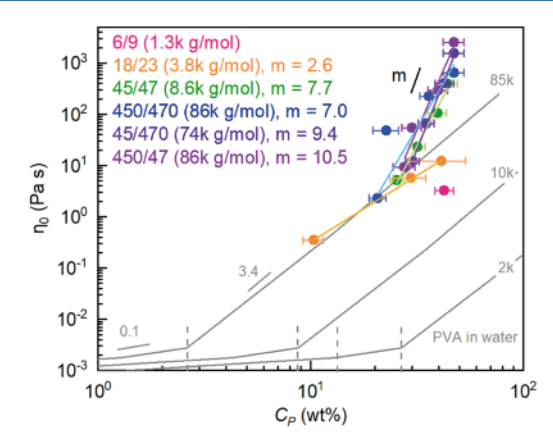


Figure 3. Zero-shear viscosity plotted as a function of the total $C_{\rm P}$ values of the coacervate in weight percent (wt %) at different $C_{\rm S}$ and chain lengths $N_{\rm anion}/N_{\rm cation}$ of 6/9, 18/23, 45/47, 450/470, 45/470, and 450/47. These data are compared to those for poly(vinyl alcohol) (PVA) at various molecular weights in water (gray lines, generalized from experimental data).⁷² Lines represent fits to the data indicating the power-law scaling. The dashed lines indicate the transition in slope, characteristic of the chain entanglement. A more detailed plot and the statistical analysis of the slopes of the coacervate samples are shown in Figures S8 and S9.

We chose two water-soluble and electrospinnable polymers, including a neutral polymer poly(vinyl alcohol) (PVA)⁷⁴ and a charged polymer chitosan,³² as examples to guide our interpretation of the correlation between viscosity and spinnability as a function of $C_{\rm P}$ (Figures 3 and S7). For both PVA and chitosan, there is a distinct change in the slope, indicating the onset of entanglements. Furthermore, with increasing N, this transition can be observed at decreasing concentrations. In general, the power-law scaling for neutral polymers is much lower than that for polyelectrolytes, with no molecular weight dependence. ^{32,74} For example, PVA showed a power-law scaling of 0.1 above C^* and 3.4 above $C_{\rm e}$, while chitosan exhibited scaling behavior of 1.3 and 6, due to charge repulsion along the chain.

We examined the zero-shear viscosity of coacervate samples as a function of C_P by preparing samples with different C_S to control Cp in the coacervate phase. Larger values for Cs lead to lower C_P, meaning that the change in polymer content, as well as the electrostatic screening from the salt ions, was expected to decrease the viscosity of the resulting coacervates. $^{53-55}$ For example, for the 45/47 samples, the addition of C_S in the range of 0.1-0.4 M resulted in coacervates with C_p of 2.2-1.3 M and a zero-shear viscosity of 400-5.2 Pa s, while for 450/470, $C_{\rm S}$ was modulated in the range of 0.3-0.6 M to produce coacervates with a similar 2.5-1.1 M range of C_P and a viscosity of 650-2.3 Pa s. The effectiveness of KBr salt can be viewed in Video S1, which demonstrates the difference in the viscosity of 45/47 coacervates prepared at 0.1 and 0.4 M KBr. The coacervates can flow freely when the vial was flipped upside down in 0.4 M KBr, whereas the sample in 0.1 M KBr was more gel-like.

We also observed that the coacervates had greater zero-shear viscosities for a given $C_{\rm P}$ compared to PVA at a similar $M_{\rm W}$ but lower viscosity than a chitosan solution of larger $M_{\rm W}$ (Figure S7). Furthermore, there appears to be a difference in the N-dependence on the magnitude of the viscosity of the coacervates as compared with traditional polymer solutions. For example, at a $C_{\rm P}$ of 30 wt %, all of the coacervates had a

zero-shear viscosity close to 10 Pa s, regardless of N. In contrast, the viscosity of PVA spans 4 orders of magnitude over the same N range. We believe that this is because of the strong associative interactions that drive coacervate formation. Even for our oligomeric coacervate sample ($M_{\rm W,coacervate}^* \sim 1.3~{\rm kg/mol}$), the viscosity was more than 2 orders of magnitude greater than for PVA of 2 kg/mol. Thus, the electrostatic interactions are the main contributor to the viscosity for coacervates and are indicative of the slow relaxation of associating polymers, rather than topological chain entanglements. Our hypothesis is that these strong electrostatic interactions are sufficient to facilitate the formation of a continuous fiber jet, even for very short oligomers.

While we did not observe a sharp slope transition on our viscosity plots for any of our coacervates samples, we did observe a change in the slope when comparing the data for the system of 20-mers to those with longer-chain lengths (Figures 3 and S8a,b). A statistical analysis based on a two-tailed, Student's t-test with p < 0.05 confirmed that the data for the 20-mers system was statistically different from that of the longer polymers, while there was no significant statistical difference between 50- and 500-mers (Figure S8c). It is also noteworthy that for the shorter oligomeric systems, a more detailed analysis was limited by the number of data points. Compared with the mismatched systems, the viscosity profiles of the matched 50-mers were significantly different from 450/47, and the matched 500-mers were significantly different from both mismatched systems.

Coacervates and Polymer Chain Entanglement. As we were unable to observe clear evidence of chain entanglement based on the analysis of the viscosity vs C_p behavior of our samples (Figure 3), we decided to couple our observations of the changes in the power-law slope behavior with theoretical predictions for the entanglement concentration. Whether there were entanglements or not, the self-assembly mechanism requires that interchain electrostatic interactions are present to form a coacervate phase. Therefore, one would expect that the concentration of the polymer present in the coacervate should be above $C^{*,78}$

Using the parameters for PMMA in a good solvent, 23 we calculated the threshold values of C^* , C_e , and C_{fiber} as a function of C_p and M_W , coacervate* as well as N (solid lines in Figure 4). We also plotted the data for our various coacervate systems using the calculated values of $M_{W,coacervate}$ *, where $M_{W,coacervate}$ * is defined as the weight average molecular weight of coacervates based on the M_N of the individual polymers, ignoring polydispersity and omitting the counterions for both polyelectrolytes (eq 1 and Table 1). Our calculations suggest that all of the coacervates had polymer concentrations that were near or above C*, as would be expected for a complex coacervate. For instance, the concentration of our shortest oligomer coacervate was 7% lower than the estimated C*, which is not likely to be a significant difference given the assumptions used and the general nature of the calculation. Furthermore, the polymer chains must experience some level of overlap to allow for the electrostatic complexation that drives phase separation.

From a classic polymer physics standpoint, there is a minimum molecular weight $(M_{\rm C})$ or N for polymers to entangle. $M_{\rm C}$ for PMMA is $M_{\rm W} \sim 15$ kg/mol, which is similar to coacervates with an average $N \sim 60$. Thus, we expect that coacervates comprised of oligomers, 20-mers, and 50-mers should not be able to achieve physical entanglements at any

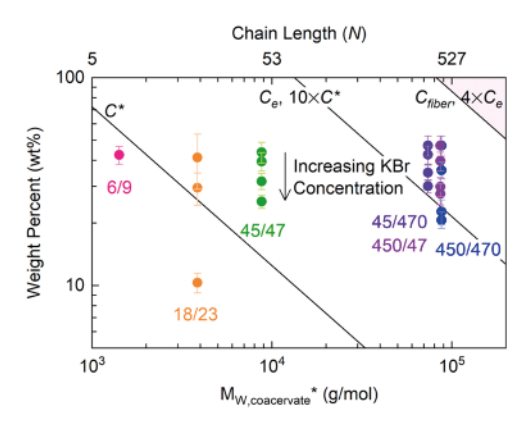


Figure 4. Log-log plot of polymer concentration (C_P , wt %) ν s average molecular weight ($M_{W,coacervate}^*$, g/mol, bottom axis) or chain length (N, top axis) for coacervates with increasing chain length (N) and salt concentration (C_S). Estimation of the overlap concentration (C^*), entanglement concentration (C_e), and onset concentrations to form fibers (C_{fiber}) was calculated using the Kuhn length for poly(methyl methacrylate) (PMMA) in a θ solvent. ^{23,52} The pink shading indicates conditions above $4 \times C_e$, corresponding to the traditional threshold for electrospinnability.

concentration. Specifically, 45/47 was 70–80% lower than $C_{\rm e}$, and 18/23 was ~90% lower than $C_{\rm e}$ (Figure 4). It should again be noted that $C_{\rm p}$ is modulated by $C_{\rm S}$, meaning that a lower $C_{\rm S}$ could be used to produce coacervates with a higher $C_{\rm p}$ to potentially affect the spinnability.

We expected that the longer-chain 500-mer polymers had the best chance to be entangled, though the samples might not achieve the $4 \times C_e$ threshold traditionally considered necessary for electrospinning. While it might be expected that the presence of such entanglements could contribute to the relatively high-viscosity dependence on C_p for the long 500mer systems, a larger slope in the viscosity scaling relationship was not observed for this longest polymer system (Figures 3 and S8). Additionally, no Cp reached the traditionally predicted C_{fiber} at their $M_{\text{W,coacervate}}$ *. In other words, from a traditional standpoint, none of our coacervates systems of matched 450/470 or mismatched systems of 450/47 and 47/ 450 would be predicted to be electrospinnable. In addition to the polymethacroloyl system considered in this work, our group has previously reported the successful electrospinning of two other polymer systems: PSS/PDADMAC ($M_{W,coacervate}^* \sim 310 \text{ kg/mol}$) and hyaluronic acid/chitosan ($M_{W,coacervate}^*$ ~ 200 kg/mol).⁴⁶ Using the parameters for PMMA, we estimate that the polymers in both of these systems were entangled but did not reach the C_{fiber} threshold.

Electrospinning Complex Coacervates. The goal of this study was to demonstrate whether the associative electrostatic interactions that drive complex coacervation can circumvent the traditional criteria for polymer electrospinnability, *i.e.*, the presence of sufficient entanglements. While conventional electrospinnable polymeric solutions require long and entangled polymers, we sought to determine the lower limit of polymer chain length for electrospinnable complex coacervates. We explored the electrospinnability for each of our coacervate systems as a function of the as-prepared $C_{\rm S}$ as a way of varying the $C_{\rm P}$.

To prepare a spinnable coacervate solution, the C_P and viscosity were key and achieved by modulating C_S for different N combinations. For coacervates formed from the longest polymers, $N \sim 500$, the electrospinnable as-prepared C_S , given

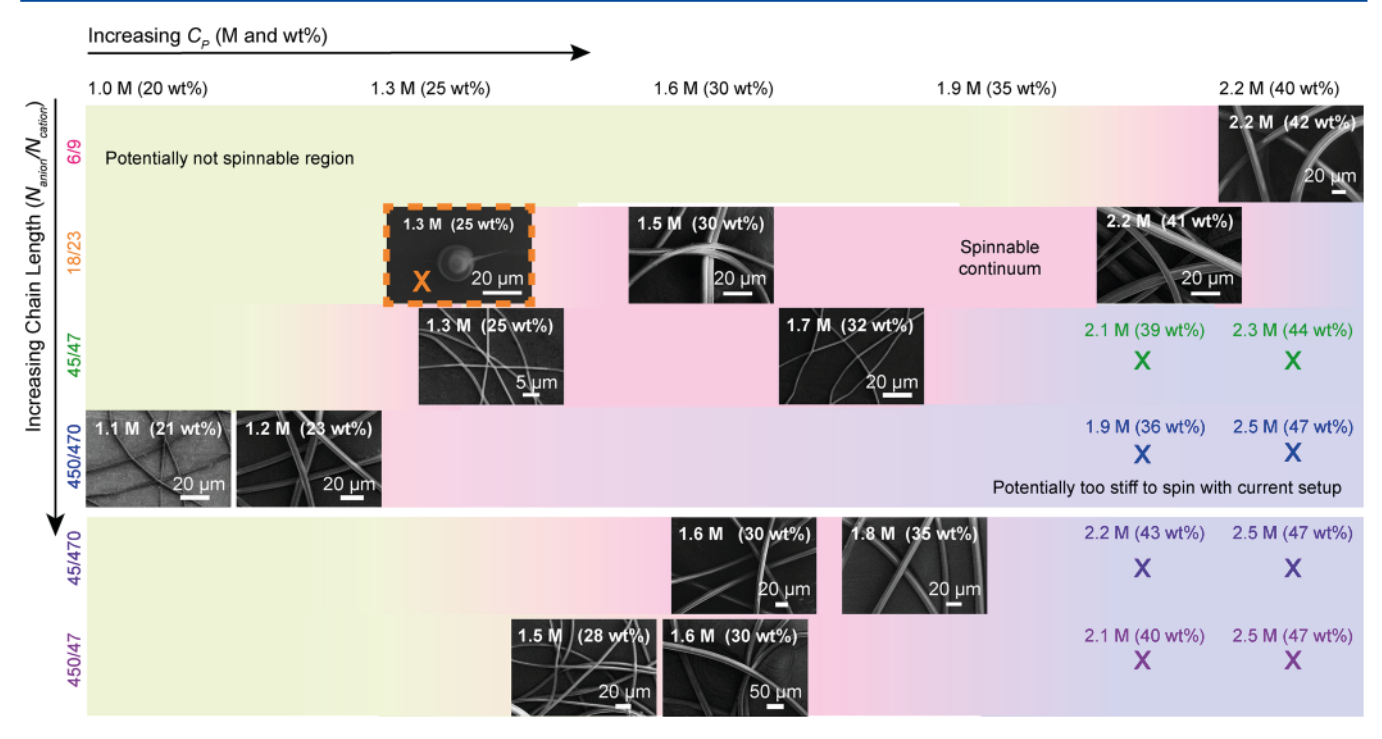


Figure 5. Schematic representation of the phase behavior and spinnability of complex coacervates as a function of polymer chain length N and the C_P in the coacervate. Scanning electron micrographs highlight conditions where electrospun polyelectrolyte complex fibers were obtained. Pink regions indicate conditions assumed to be electrospinnable between the tested samples. Blue regions at higher C_P indicate conditions where coacervates formed but were too stiff to extrude through the spinneret in our current setup. In contrast, green regions indicate conditions at lower C_P where no fiber formation was observed given the operating conditions used in this study, potentially due to the low viscosity/fast relaxation of the samples and/or where coacervation did not take place (i.e., a single-phase solution was observed). An "X" indicates that a sample was prepared but failed to electrospin into fibers. The orange "X" in the dashed line—boxed sample in the 18/23 system indicates a transition point thought to represent the onset of fiber formation, which is in between electrosprayed droplets and continuous fiber formation. The electrospinning apparatus conditions were held constant for all samples (see the Materials and Methods section for details). The highlighted regions were determined from only one set of experiments using consistent apparatus conditions. Coacervate electrospinnability vs the as-prepared C_S is displayed in Figure S10, while Figure S11 maps the coacervate spinnability onto the binodal curves for the various samples.

our apparatus parameters, was determined to be 0.5-0.6 M KBr experimentally. The polymeric interactions under these conditions were adequate to facilitate the formation of smooth, continuous fibers in this range of Cp, as highlighted in pink in Figure 5. At higher C_p (lower C_s), a solid precipitate or gel would form, meaning that the complexes were too stiff to be electrospun using our current setup (highlighted in blue). It should be noted that these stiff complexes could potentially be electrospun using a setup designed for more viscous solutions, 79,80 whereas our focus in this paper was on chainlength effects separate from considerations associated with electrospinning operational parameters. With higher C_S , the formation of a coacervate phase was challenging and/or the polymeric interactions in the coacervates were too weak to facilitate fiber formation, as highlighted in green. While the successful electrospinning of our longest-chain coacervates might not have been predicted based on the traditional C_{fiber} threshold, our predictions did indicate the presence of some level of entanglements. Thus, while this result indicates that electrostatic interactions can reduce the level of entanglements needed to facilitate electrospinning, it does not demonstrate whether or not such associative interactions could replace entanglements entirely.

Coacervates prepared from polymers of mismatched N provide an interesting bridge from coacervates formed entirely from long νs short polymers. For the aforementioned electrospinnable system of long 500-mers, the polycation and

polyanion had the potential to be entangled with each other, in addition to experiencing associative ion-pairing interactions. In contrast, for coacervates formed from polymers with mismatched chain lengths (i.e., 450/47, 47/450), only the longer polymer would have the potential to be entangled (Figure S9). Despite this further reduction in the potential number of entanglements, we were able to successfully electrospun fibers from these mismatched coacervate samples, albeit at a lower salt and polymer concentration than for the 500-mers, owing to the dominance of the shorter polymers on the phase behavior (Figures 5, S11, and S12).

To further probe the role of entanglements in a mismatched system, we prepared samples containing the long ~500-mer polymer at the same C_p as the mismatched coacervates but substituted the shorter polymer for a charge equivalent concentration of monomers. As our previous experiments with this formulation had not resulted in the formation of a coacervate phase, this sample served to test the role of entanglements without the presence of multivalent electrostatic interactions that could bridge multiple polymer chains. Despite the presence of some chain entanglement, electrospinning experiments failed to yield continuous fibers from these solutions. This result highlighted the importance of cooperative, multivalent interactions between oppositely charged polymers in achieving the electrospinnability of the lengthmismatched coacervates, demonstrating that the electrospinnability of coacervates is fundamentally different from

traditional solutions of linear polymers or mixtures of polyelectrolytes with polymers. The electrospinnability of coacervates comes from the associative electrostatic interactions rather than merely an entangled high-molecular-weight polymer.

Moving on to consider coacervates formed from shorter polymers and even oligomers for which entanglements were not physically possible, it was very exciting to observe continuous and cylindrical fiber formation for all of our different N samples, including oligomeric coacervates, with lower $C_{\rm S}$ being needed for shorter N (Figures 5 and S11). While our control experiments demonstrated that a mixture of oppositely charged monomers could neither form a coacervate nor electrospin, the threshold level of interactions necessary to facilitate both phase separation and electrospinning is somewhere in the 1 < N < 6/9 range.

Although we were not able to definitively identify a lower limit on N for the electrospinnability of our methacryloylbased coacervates, our results highlight a connection between the chain length and the minimum C_P needed to electrospin. This broad trend can be envisaged based on the data shown in Figures 5 and S11. However, we will highlight one particular example for coacervates formed with $N_{\rm anion}/N_{\rm cation}$ of 18/23. We observed a transition indicative of the onset of fiber formation, i.e., a transition from smooth continuous fibers to discontinuous short fibers extending from electrosprayed droplets going from an as-prepared C_S of 0.1-0.2 M. This represented a decrease in C_p from 1.6 M on a monomer basis (29.6 wt %) to 1.3 M on a monomer basis (10.3 wt %) and a decrease in the viscosity from 5.1 to 0.4 Pa s. This result is in contrast with fibers formed from 500-mer coacervates that were prepared at a C_S of 0.6 M, for which C_P was 1.1 M on a monomer basis (20.7 wt %). However, the ability to use polymer chain length to further modulate the necessary C_p in the coacervates will be limited by the overall phase envelope and the fact that chain-length effects tend to attenuate above N $\sim 200-500.^{47,68,81}$ This complex interplay of variables suggests that a more universal measure of coacervate electrospinnability, such as one based on a more detailed rheological analysis than simple viscosity measurements, could be very useful to simplify efforts related to electrospinning coacervates. However, such a study is beyond the scope of the current work.

These results represent the first time that electrostatic interactions associated with complex coacervation have been evaluated as a mechanism to drive electrospinning. Previous reports have confirmed that associative interactions can indeed drive electrospinning of supramolecules, ¹⁷ for example, hydrogen bonding facilitated the electrospinning of P4VP³³ and of self-associating cyclodextrins^{36–39} and tannic acid. ⁴⁰ While extending into the size scale of small molecules, our work highlights the way in which the electrostatic interactions driving complex coacervation can allow for a continuum of processability, from the smallest oligomers to long-chain polymers. This fully realizes the potential for tuning chainlength-dependent material properties of the resulting fibers separately from the requirements for processing.

CONCLUSIONS

This work demonstrates that the associative electrostatic interactions that drive complex coacervation can also be used to eliminate polymer chain length and entanglement requirements for electrospinning. We bridged studies of electrospinnability with phase diagram determination and rheological

characterization using a model system of methacryloyl-based polyelectrolytes ranging in chain lengths from N < 10 to ~ 500 or molecular weights from 1 to 100 kg/mol. Smooth continuous fibers were successfully electrospun even from coacervates formed from oligomers. We observed an interplay between electrospinnability, chain length, and the concentration of the polymer in the coacervate. Our ability to electrospin oligomers via complex coacervation decouples the polymer electrospinnability from the molecular weight requirements, which shed light on designing new solid materials, which were deemed impossible in the past.

ASSOCIATED CONTENT

Supporting Information

The Supporting Information is available free of charge at https://pubs.acs.org/doi/10.1021/acs.macromol.1c00397.

Chemical reactions, 1H NMR spectra of reactants and products related to monomer and polymer syntheses, molecular weight ($M_{W,coacervate}^*$ and $M_{N,coacervate}^*$) calculation for coacervates, salt stability results for coacervates of various N, calibration curve for salt concentration vs conductivity, coacervate viscosity plots, entanglement plots, binodal phase separation curves, SEM micrographs of spun coacervates (PDF)

Video on the coacervate formation and viscosity comparison (Video S1) (MP4)

AUTHOR INFORMATION

Corresponding Authors

Sarah L. Perry — Department of Chemical Engineering,
University of Massachusetts, Amherst, Amherst,
Massachusetts 01003-930, United States; orcid.org/
0000-0003-2301-6710; Email: perrys@engin.umass.edu
Jessica D. Schiffman — Department of Chemical Engineering,
University of Massachusetts, Amherst, Amherst,
Massachusetts 01003-930, United States; orcid.org/
0000-0002-1265-5392; Email: schiffman@ecs.umass.edu

Authors

Xiangxi Meng — Department of Chemical Engineering, University of Massachusetts, Amherst, Amherst, Massachusetts 01003-930, United States; orcid.org/ 0000-0003-3886-7892

Yifeng Du — Department of Polymer Science & Engineering, University of Massachusetts, Amherst, Amherst, Massachusetts 01003-930, United States

Yalin Liu — Department of Chemical Engineering, University of Massachusetts, Amherst, Amherst, Massachusetts 01003-930, United States; orcid.org/0000-0002-1513-1922

E. Bryan Coughlin – Department of Polymer Science & Engineering, University of Massachusetts, Amherst, Amherst, Massachusetts 01003-930, United States; ⊙ orcid.org/ 0000-0001-7065-4366

Complete contact information is available at: https://pubs.acs.org/10.1021/acs.macromol.1c00397

Notes

The authors declare no competing financial interest.

ACKNOWLEDGMENTS

The authors thank Jacob Schladenhauffen for the preliminary experiments. X.M. acknowledges the support of the National

Science Foundation NRT-SMLS program (DGE-1545399). The authors acknowledge the support of the National Science Foundation (NSF CMMI-1727660) and a UMass Amherst Faculty Research Grant, as well as facilities at the W.M. Keck Center for Electron Microscopy. E.B.C. and Y.D. gratefully acknowledge the financial support from the Army Research Office through Grant W911NF-17-1-0568 and W911NF-19-1-0286.

■ REFERENCES

- (1) Ramakrishna, S.; Fujihara, K.; Teo, W.-E.; Yong, T.; Ma, Z.; Ramaseshan, R. Electrospun Nanofibers: Solving Global Issues. *Mater. Today* 2006, 9, 40–50.
- (2) Mirjalili, M.; Zohoori, S. Review for Application of Electrospinning and Electrospin Nanofibers Technology in Textile Industry. *J. Nanostruct. Chem.* 2016, 6, 207–213.
- (3) Persano, L.; Camposeo, A.; Tekmen, C.; Pisignano, D. Industrial Upscaling of Electrospinning and Applications of Polymer Nanofibers: a Review. *Macromol. Mater. Eng.* 2013, 298, 504–520.
- (4) Mingjun, C.; Youchen, Z.; Haoyi, L.; Xiangnan, L.; Yumei, D.; Bubakir, M. M.; Weimin, Y. An Example of Industrialization of Melt Electrospinning: Polymer Melt Differential Electrospinning. *Adv. Ind. Eng. Polym. Res.* 2019, 2, 110–115.
- (5) Jeong, S. I.; Krebs, M. D.; Bonino, C. A.; Samorezov, J. E.; Khan, S. A.; Alsberg, E. Electrospun Chitosan—Alginate Nanofibers with in SituPolyelectrolyte Complexation for Use as Tissue Engineering Scaffolds. *Tissue Eng., Part A* 2011, 17, 59—70.
- (6) Matthews, J. A.; Wnek, G. E.; Simpson, D. G.; Bowlin, G. L. Electrospinning of Collagen Nanofibers. *Biomacromolecules* 2002, 3, 232–238.
- (7) Yoo, H. S.; Kim, T. G.; Park, T. G. Surface-Functionalized Electrospun Nanofibers for Tissue Engineering and Drug Delivery. *Adv. Drug Delivery Rev.* 2009, *61*, 1033–1042.
- (8) Dobosz, K. M.; Kolewe, K. W.; Schiffman, J. D. Green Materials Science and Engineering Reduces Biofouling: Approaches for Medical and Membrane-Based Technologies. *Front. Microbiol.* 2015, 6, No. 196
- (9) Gopal, R.; Kaur, S.; Ma, Z.; Chan, C.; Ramakrishna, S.; Matsuura, T. Electrospun Nanofibrous Filtration Membrane. *J. Membr. Sci.* 2006, 281, 581–586.
- (10) Jung, J.-W.; Lee, C.-L.; Yu, S.; Kim, I.-D. Electrospun Nanofibers as a Platform for Advanced Secondary Batteries: A Comprehensive Review. J. Mater. Chem. A 2016, 4, 703-750.
- (11) Dong, Z.; Kennedy, S. J.; Wu, Y. Electrospinning Materials for Energy-Related Applications and Devices. *J. Power Sources* 2011, 196, 4886–4904.
- (12) Schiffman, J. D.; Schauer, C. L. A Review: Electrospinning of Biopolymer Nanofibers and Their Applications. *Polym. Rev.* 2008, 48, 317–352.
- (13) Anton, F. Process and Apparatus for Preparing Artificial Threads. US1,975,504A, 1934.
- (14) Doshi, J.; Reneker, D. H. Electrospinning Process and Applications of Electrospun Fibers. J. Electrost. 1995, 35, 151–160.
- (15) Taylor, G. Disintegration of Water Drops in an Electric Field. Proc. R. Soc. London, Ser. A 1964, 280, 383-397.
- (16) Taylor, G. Electrically Driven Jets. Proc. R. Soc. London, Ser. A 1969, 313, 453-475.
- (17) Ewaldz, E.; Brettmann, B. Molecular Interactions in Electrospinning: From Polymer Mixtures to Supramolecular Assemblies. ACS Appl. Polym. Mater. 2019, 1, 298–308.
- (18) Rutledge, G. C.; Fridrikh, S. V. Formation of Fibers by Electrospinning. Adv. Drug Delivery Rev. 2007, 59, 1384–1391.
- (19) Hohman, M. M.; Shin, M.; Rutledge, G.; Brenner, M. P. Electrospinning and Electrically Forced Jets. I. Stability Theory. *Phys. Fluids* 2001, *13*, 2201–2220.
- (20) Xue, J.; Wu, T.; Dai, Y.; Xia, Y. Electrospinning and Electrospun Nanofibers: Methods, Materials, and Applications. *Chem. Rev.* 2019, 119, 5298-5415.

- (21) De Gennes, P. G. Dynamics of Entangled Polymer Solutions. I. the Rouse Model. *Macromolecules* 1976, 9, 587–593.
- (22) Sperling, L. H. Introduction to Physical Polymer Science; John Wiley & Sons, 2005.
- (23) Rubinstein, M.; Colby, R. H. Polymer Physics; Oxford University Press, 2003.
- (24) Regev, O.; Vandebril, S.; Zussman, E.; Clasen, C. The Role of Interfacial Viscoelasticity in the Stabilization of an Electrospun Jet. *Polymer* 2010, *51*, 2611–2620.
- (25) McKee, M. G.; Wilkes, G. L.; Colby, R. H.; Long, T. E. Correlations of Solution Rheology with Electrospun Fiber Formation of Linear and Branched Polyesters. *Macromolecules* 2004, 37, 1760–1767.
- (26) Klossner, R. R.; Queen, H. A.; Coughlin, A. J.; Krause, W. E. Correlation of Chitosan's Rheological Properties and Its Ability to Electrospin. *Biomacromolecules* 2008, *9*, 2947–2953.
- (27) Chen, H.; Snyder, J. D.; Elabd, Y. A. Electrospinning and Solution Properties of Nafion and Poly(Acrylic Acid). *Macromolecules* 2008, 41, 128–135.
- (28) Kong, L.; Ziegler, G. R. Molecular Entanglement and Electrospinnability of Biopolymers. *J. Visualized Exp.* 2014, 91, No. e51933.
- (29) Rieger, K. A.; Birch, N. P.; Schiffman, J. D. Designing Electrospun Nanofiber Mats to Promote Wound Healing A Review. *J. Mater. Chem. B* 2013, 1, 4531–4541.
- (30) Shenoy, S. L.; Bates, W. D.; Frisch, H. L.; Wnek, G. E. Role of Chain Entanglements on Fiber Formation During Electrospinning of Polymer Solutions: Good Solvent, Non-Specific Polymer—Polymer Interaction Limit. *Polymer* 2005, 46, 3372—3384.
- (31) Saquing, C. D.; Tang, C.; Monian, B.; Bonino, C. A.; Manasco, J. L.; Alsberg, E.; Khan, S. A. Alginate-Polyethylene Oxide Blend Nanofibers and the Role of the Carrier Polymer in Electrospinning. *Ind. Eng. Chem. Res.* 2013, 52, 8692–8704.
- (32) Koski, A.; Yim, K.; Shivkumar, S. Effect of Molecular Weight on Fibrous PVA Produced by Electrospinning. *Mater. Lett.* 2004, 58, 493–497.
- (33) Wang, X.; Pellerin, C.; Bazuin, C. G. Enhancing the Electrospinnability of Low Molecular Weight Polymers Using Small Effective Cross-Linkers. *Macromolecules* 2016, 49, 891–899.
- (34) Chen, Y. Z.; Peng, P.; Guo, Z.-X.; Yu, J.; Zhan, M. S. Effect of Hyperbranched Poly(Ester Amine) Additive on Electrospinning of Low Concentration Poly(Methyl Methacrylate) Solutions. *J. Appl. Polym. Sci.* 2010, 115, 3687–3696.
- (35) Hunley, M. T.; Harber, A.; Orlicki, J. A.; Rawlett, A. M.; Long, T. E. Effect of Hyperbranched Surface-Migrating Additives on the Electrospinning Behavior of Poly(Methyl Methacrylate). *Langmuir* 2008, 24, 654–657.
- (36) Celebioglu, A.; Uyar, T. Cyclodextrin Nanofibers by Electrospinning. Chem. Commun. 2010, 46, 6903-6905.
- (37) Celebioglu, A.; Kayaci-Senirmak, F.; İpek, S.; Durgun, E.; Uyar, T. Polymer-Free Nanofibers From Vanillin/Cyclodextrin Inclusion Complexes: High Thermal Stability, Enhanced Solubility and Antioxidant Property. *Food Funct.* 2016, 7, 3141–3153.
- (38) Celebioglu, A.; Uyar, T. Electrospinning of Polymer-Free Nanofibers From Cyclodextrin Inclusion Complexes. *Langmuir* 2011, 27, 6218–6226.
- (39) Celebioglu, A.; Uyar, T. Electrospinning of Nanofibers From Non-Polymeric Systems: Electrospun Nanofibers From Native Cyclodextrins. J. Colloid Interface Sci. 2013, 404, 1–7.
- (40) Allais, M.; Mailley, D.; Hébraud, P.; Ihiawakrim, D.; Ball, V.; Meyer, F.; Hébraud, A.; Schlatter, G. Polymer-Free Electrospinning of Tannic Acid and Cross-Linking in Water for Hybrid Supramolecular Nanofibres. *Nanoscale* 2018, 10, 9164—9173.
- (41) Sing, C. E.; Perry, S. L. Recent Progress in the Science of Complex Coacervation. Soft Matter 2020, 16, 2885-2914.
- (42) Spruijt, E.; Leermakers, F. A. M.; Fokkink, R.; Schweins, R.; van Well, A. A.; Cohen Stuart, M. A.; van der Gucht, J. Structure and Dynamics of Polyelectrolyte Complex Coacervates Studied by

- Scattering of Neutrons, X-Rays, and Light. Macromolecules 2013, 46, 4596-4605.
- (43) Liu, Y.; Winter, H. H.; Perry, S. L. Linear Viscoelasticity of Complex Coacervates. Adv. Colloid Interface Sci. 2017, 239, 46-60.
- (44) Meng, X.; Perry, S. L.; Schiffman, J. D. Complex Coacervation: Chemically Stable Fibers Electrospun From Aqueous Polyelectrolyte Solutions. ACS Macro Lett. 2017, 6, 505–511.
- (45) Meng, X.; Schiffman, J. D.; Perry, S. L. Electrospinning Cargo-Containing Polyelectrolyte Complex Fibers: Correlating Molecular Interactions to Complex Coacervate Phase Behavior and Fiber Formation. *Macromolecules* 2018, *51*, 8821–8832.
- (46) Sun, J.; Perry, S. L.; Schiffman, J. D. Electrospinning Nanofibers From Chitosan/Hyaluronic Acid Complex Coacervates. *Biomacromolecules* 2019, 20, 4191–4198.
- (47) Liu, Y.; Santa Chalarca, C. F.; Carmean, R. N.; Olson, R. A.; Madinya, J.; Sumerlin, B. S.; Sing, C. E.; Emrick, T.; Perry, S. L. Effect of Polymer Chemistry on the Linear Viscoelasticity of Polyelectrolyte Complexes. *Macromolecules* 2020, *53*, 7851–7864.
- (48) Konkolewicz, D.; Siauw, M.; Gray-Weale, A.; Hawkett, B. S.; Perrier, S. Obtaining Kinetic Information From the Chain-Length Distribution of Polymers Produced by RAFT. *J. Phys. Chem. B* 2009, 113, 7086–7094.
- (49) Perrier, S. 50th Anniversary Perspective: RAFT Polymerization—A User Guide. *Macromolecules* 2017, 50, 7433-7447.
- (50) Siauw, M.; Hawkett, B. S.; Perrier, S. Short Chain Amphiphilic Diblock Co-Oligomers via RAFT Polymerization. *J. Polym. Sci., Part A: Polym. Chem.* 2012, 50, 187–198.
- (51) Baumgaertel, M.; Winter, H. H. Determination of Discrete Relaxation and Retardation Time Spectra From Dynamic Mechanical Data. *Rheol. Acta* 1989, 28, 511–519.
- (52) Colby, R. H. Structure and Linear Viscoelasticity of Flexible Polymer Solutions: Comparison of Polyelectrolyte and Neutral Polymer Solutions. *Rheol. Acta* 2010, 49, 425–442.
- (53) Schaaf, P.; Schlenoff, J. B. Saloplastics: Processing Compact Polyelectrolyte Complexes. *Adv. Mater.* 2015, 27, 2420–2432.
- (54) Porcel, C. H.; Schlenoff, J. B. Compact Polyelectrolyte Complexes: "Saloplastic" Candidates for Biomaterials. *Biomacromolecules* 2009, 10, 2968–2975.
- (55) Wang, Q.; Schlenoff, J. B. The Polyelectrolyte Complex/Coacervate Continuum. *Macromolecules* 2014, 47, 3108-3116.
- (56) Sing, C. E.; Perry, S. L. Recent Progress in the Science of Complex Coacervation. *Soft Matter* 2020, *16*, 2885–2914.
- (57) Madinya, J. J.; Chang, L.-W.; Perry, S. L.; Sing, C. E. Sequence-Dependent Self-Coacervation in High Charge-Density Polyampholytes. *Mol. Syst. Des. Eng.* 2020, 5, 632–644.
- (58) Chollakup, R.; Beck, J. B.; Dirnberger, K.; Tirrell, M.; Eisenbach, C. D. Polyelectrolyte Molecular Weight and Salt Effects on the Phase Behavior and Coacervation of Aqueous Solutions of Poly(Acrylic Acid) Sodium Salt and Poly(Allylamine) Hydrochloride. *Macromolecules* 2013, 46, 2376–2390.
- (59) Priftis, D.; Tirrell, M. Phase Behaviour and Complex Coacervation of Aqueous Polypeptide Solutions. *Soft Matter* **2012**, *8*, 9396–9405.
- (60) Li, L.; Srivastava, S.; Andreev, M.; Marciel, A. B.; de Pablo, J. J.; Tirrell, M. V. Phase Behavior and Salt Partitioning in Polyelectrolyte Complex Coacervates. *Macromolecules* 2018, *51*, 2988–2995.
- (61) Akkaoui, K.; Yang, M.; Digby, Z. A.; Schlenoff, J. B. Ultraviscosity in Entangled Polyelectrolyte Complexes and Coacervates. *Macromolecules* 2020, 53, 4234–4246.
- (62) Chang, L.-W.; Lytle, T. K.; Radhakrishna, M.; Madinya, J. J.; Vélez, J.; Sing, C. E.; Perry, S. L. Sequence and Entropy-Based Control of Complex Coacervates. *Nat. Commun.* 2017, 8, No. 1273.
- (63) Lytle, T. K.; Chang, L.-W.; Markiewicz, N.; Perry, S. L.; Sing, C. E. Designing Electrostatic Interactions via Polyelectrolyte Monomer Sequence. ACS Cent. Sci. 2019, 5, 709—718.
- (64) Sing, C. E. Development of the Modern Theory of Polymeric Complex Coacervation. *Adv. Colloid Interface Sci.* 2017, 239, 2–16.

- (65) Priftis, D.; Laugel, N.; Tirrell, M. Thermodynamic Characterization of Polypeptide Complex Coacervation. *Langmuir* 2012, 28, 15947–15957.
- (66) Salehi, A.; Larson, R. G. A Molecular Thermodynamic Model of Complexation in Mixtures of Oppositely Charged Polyelectrolytes with Explicit Account of Charge Association/Dissociation. *Macromolecules* 2016, 49, 9706–9719.
- (67) Manning, G. S. Limiting Laws and Counterion Condensation in Polyelectrolyte Solutions I. Colligative Properties. *J. Chem. Phys.* 1969, 51, 924–933.
- (68) Spruijt, E.; Westphal, A. H.; Borst, J. W.; Cohen Stuart, M. A.; van der Gucht, J. Binodal Compositions of Polyelectrolyte Complexes. *Macromolecules* 2010, 43, 6476–6484.
- (69) Koga, S.; Williams, D. S.; Perriman, A. W.; Mann, S. Peptide—Nucleotide Microdroplets as a Step Towards a Membrane-Free Protocell Model. *Nat. Chem.* 2011, 3, 720–724.
- (70) Huang, Z.-M.; Zhang, Y. Z.; Kotaki, M.; Ramakrishna, S. A Review on Polymer Nanofibers by Electrospinning and Their Applications in Nanocomposites. *Compos. Sci. Technol.* 2003, 63, 2223–2253.
- (71) Li, L.; Srivastava, S.; Meng, S.; Ting, J. M.; Tirrell, M. Effects of Non-Electrostatic Intermolecular Interactions on the Phase Behavior of pH-Sensitive Polyelectrolyte Complexes. *Macromolecules* 2020, 53, 7835–7844.
- (72) Pakravan, M.; Heuzey, M.-C.; Ajji, A. A Fundamental Study of Chitosan/PEO Electrospinning. *Polymer* 2011, 52, 4813–4824.
- (73) Son, W. K.; Youk, J. H.; Lee, T. S.; Park, W. H. The Effects of Solution Properties and Polyelectrolyte on Electrospinning of Ultrafine Poly(Ethylene Oxide) Fibers. *Polymer* 2004, 45, 2959–2966
- (74) Bercea, M.; Morariu, S.; Rusu, D. *In Situ* Gelation of Aqueous Solutions of Entangled Poly(Vinyl Alcohol). *Soft Matter* 2013, 9, 1244–1253.
- (75) Spruijt, E.; Cohen Stuart, M. A.; van der Gucht, J. Linear Viscoelasticity of Polyelectrolyte Complex Coacervates. *Macromolecules* 2013, 46, 1633–1641.
- (76) Spruijt, E.; Sprakel, J.; Lemmers, M.; Stuart, M. A. C.; van der Gucht, J. Relaxation Dynamics at Different Time Scales in Electrostatic Complexes: Time-Salt Superposition. *Phys. Rev. Lett.* 2010, 105, No. 208301.
- (77) van der Gucht, J.; Spruijt, E.; Lemmers, M.; Stuart, M. A. C. Polyelectrolyte Complexes: Bulk Phases and Colloidal Systems. *J. Colloid Interface Sci.* 2011, 361, 407–422.
- (78) Marciel, A. B.; Srivastava, S.; Tirrell, M. V. Structure and Rheology of Polyelectrolyte Complex Coacervates. *Soft Matter* 2018, 14, 2454–2464.
- (79) Um, I. C.; Fang, D.; Hsiao, B. S.; Okamoto, A.; Chu, B. Electro-Spinning and Electro-Blowing of Hyaluronic Acid. *Biomacromolecules* 2004, *5*, 1428–1436.
- (80) Wang, X.; Um, I. C.; Fang, D.; Okamoto, A.; Hsiao, B. S.; Chu, B. Formation of Water-Resistant Hyaluronic Acid Nanofibers by Blowing-Assisted Electro-Spinning and Non-Toxic Post Treatments. *Polymer* 2005, 46, 4853–4867.
- (81) Qin, J.; Priftis, D.; Farina, R.; Perry, S. L.; Leon, L.; Whitmer, J.; Hoffmann, K.; Tirrell, M.; de Pablo, J. J. Interfacial Tension of Polyelectrolyte Complex Coacervate Phases. *ACS Macro Lett.* 2014, 3, 565–568.